Journal of Fluids and Structures 17 (2003) 1161–1180

JOURNAL OF FLUIDS AND STRUCTURES

www.elsevier.nl/locate/jnlabr/yjfls

Methods of fluid–structure coupling in frequency and time domains using linearized aerodynamics for turbomachinery

D.-M. Tran*, C. Liauzun, C. Labaste[1]

Structural Dynamics and Coupled Systems Department, Office National d'Études et de Recherches Aérospatiales B.P. 72, 29 avenue de la Division Leclerc, 92322 Châtillon Cedex, France

Received 16 February 2002; accepted 18 April 2003

Abstract

Two methods of fluid–structure coupling for turbomachinery are presented, the first one in the frequency domain and the second in both frequency and time domains. In both methods, the structure and the fluid are assumed to have circumferential cyclic symmetric properties and the unsteady aerodynamic forces are assumed to be linear in terms of the structural displacements. The motion equation of the reference sector in the travelling wave coordinates is projected on the complex eigenmodes for each phase number. The generalized unsteady aerodynamic forces are computed by solving the Euler equations and by assuming the structural motion to be harmonic with a constant phase angle between two adjacent sectors. In the frequency domain, the complex, nonlinear eigenvalue problem for the aeroelastic stability analysis is solved iteratively either by the double scanning method or by using Karpel's minimum state smoothing of the aerodynamic coefficient matrix. In the time domain, Karpel's smoothing method is used to obtain an approximation of the generalized unsteady aerodynamic forces by means of auxiliary state variables. These coupling methods are tested on a compressor blade row and the good agreement obtained between their results and those of the direct coupling method shows that the proposed numerical methods, already used in aircraft applications, are adapted to turbomachinery.

1. Introduction

This paper is concerned with the coupled fluid–structure dynamic analysis of turbomachinery. The structure consists of a rotating bladed disk submitted to the unsteady aerodynamic forces exerted by the fluid, which are themselves generated by the structural motion. In this paper, the structure and the fluid are assumed to have a perfect circumferential cyclic symmetry, so that the classical reduction of the analysis to only one reference sector can be applied. The case of mistuned bladed disks in which the cyclic symmetry is slightly broken is not considered. The properties of structures with cyclic symmetry are obtained from the wave propagation theory in periodic structures (Brillouin, 1946; Mead, 1975; Orris and Petyt, 1974; Thomas, 1979; Wildheim, 1979) and can also be derived from the theory of finite groups (Miller, 1981; Valid and Ohayon, 1985). They have been applied to rotating systems such as flexible rotors or disk–blade assemblies (Géradin and Kill, 1986; Mézière, 1994; Jacquet-Richardet et al., 1996) and can be combined with model order reduction methods such as component mode synthesis (Henry, 1980; Elhami et al., 1993; Tran, 2000, 2001).

Aeroelasticity formulations for turbomachinery applications, i.e., the coupling of the structural dynamic and the unsteady aerodynamic models, were reviewed by Crawley (1988) and Marshall and Imregun (1996). The structural

*Corresponding author. Tel.: +33-1-46-73-46-32; fax: +33-1-46-73-41-43.
E-mail addresses: minh.tran_duc@onera.fr (D.-M. Tran).
[1] Present address: Office National d'Études et de Recherches Aérospatiales, Centre du Fauga-Mauzac, 31410 Mauzac, France.

0889-9746/03/$ - see front matter
doi:10.1016/S0889-9746(03)00068-9

motion equation is usually projected on structural modes. Several types of modes are proposed to represent the structural dynamic model and to compute the unsteady aerodynamic forces: reference sector travelling wave modes (Jacquet-Richardet and Henry, 1994; Tran et al., 2001), structure standing wave modes (Lalanne and Touratier, 1998; Lalanne et al., 1998) isolated reference sector component modes (Jacquet-Richardet and Dal-Ferro, 1995), isolated disk and blade component modes (Berthillier et al., 1997, 1998), etc.

Using the cyclic symmetry properties, the study of the whole structure comes down to that of the reference sector by applying the appropriate boundary conditions for each phase number. After finite element discretization, we obtain the equation of motion of the reference sector in the travelling wave coordinates in which the rotational effects are taken into account. For each phase number, the complex modes of the reference sector are computed using the symmetric cyclic boundary conditions and by neglecting the damping and gyroscopic matrices. The displacements of the reference sector are then expressed as a linear combination of the complex modes and the motion equations are projected on these modes to obtain a reduced system. Other projection bases such as Craig and Bampton's (1968) can be used, for example, to take into account structural nonlinearities.

The unsteady aerodynamic forces are assumed to depend linearly on the structural displacements and velocities and they are expressed in terms of those induced by the modes. The mode-induced aerodynamic forces are computed by using an aerodynamic code (solving the Euler equations) with the assumption of harmonic motion of the modes, for an inter-blade phase angle and a number of reduced oscillation frequencies. In the proposed indirect coupling methods, the aerodynamic forces are determined only once at the beginning of the simulation and the structural motion does not interact directly on the aerodynamic forces but only via the structural modes, thanks to the hypotheses of linearized aerodynamics and harmonic motion. These assumptions are removed in the direct coupling method where the structural motion equation, projected or not on the modes, and the fluid equations are solved alternately at each time step, with the data transferred from one computation to the next one (as boundary conditions or pressure load) via the fluid–structure interface (Maman and Farhat, 1995; Farhat et al., 1995; Jacquet-Richardet and Rieutord, 1998; Sayma et al., 2000; Grisval and Liauzun, 1999, 2000). Another possibility would consist in solving simultaneously the motion equations of the structure and the fluid by using the same type of discretization and numerical solution methods for both domains, but this fully coupled technique requires a lot of computational time and is not easy to handle.

In the coupling methods used here, the projection of the mode-induced aerodynamic forces on the modes provides a complex matrix of aerodynamic coefficients whose product with the modal coordinates represents the generalized aerodynamic forces in the frequency domain. Introducing the aerodynamic coefficient matrix in the reduced system for the stability analysis, we obtain a nonlinear eigenvalue system in which the matrix depends on the unknown eigenvalue. This flutter equation is solved by using two well-known iterative techniques that have been used for the aeroelastic stability of aircraft (Mastroddi and Gennaretti, 2001). The first one is the double scanning method (Dat and Meurzec, 1969) (also called *p–k* method) in which the unknown eigenvalues are replaced by their imaginary parts when evaluating the aerodynamic coefficient matrix. The second one uses the frequency-domain expression of the aerodynamic coefficient matrix obtained from Karpel's minimum state smoothing method based on an approximation by rational functions (Karpel, 1982; Roberts, 1991; Poirion, 1995). The stability of the system is determined by considering the damping of each aeroelastic mode.

In the time domain, the generalized aerodynamic forces for an arbitrary motion cannot be expressed as the product of the aerodynamic coefficient matrix with the generalized coordinates. Karpel's minimum state smoothing of the aerodynamic coefficient matrix is used to obtain a time-domain approximation of the generalized aerodynamic forces by means of auxiliary state variables. The reduced coupled system is solved by using a Newmark second-order time scheme (Newmark, 1959; Bathe, 1996). Structural nonlinearities such as friction or free-play can then be taken into account. This numerical strategy is applied to a compressor blade for different configurations (phase numbers, rotation speeds). The results are compared between the proposed methods and also to those obtained using the direct coupling method.

This paper is organized as follows: in Section 2, the properties of structures with cyclic symmetry are reviewed. The coupling method based on the projection on the complex modes is presented in Section 3. The computation of the generalized unsteady aerodynamic forces is described in Section 4. The solution of the coupled system using the double scanning method and the minimum state smoothing method is presented in Section 5. Finally, a numerical example is studied in Section 6.

2. Structure with cyclic symmetry

2.1. Reduction to the reference sector

A structure with cyclic symmetry is composed of N identical sectors $S_0, S_1, \ldots, S_{N-1}$ which close up on themselves to form a circular system. The whole structure is obtained by $N-1$ repeated rotations of a reference sector S_0 through the angle $\beta = 2\pi/N$. Each sector is limited by a left frontier L_l and a right frontier L_r with the adjacent sectors. The fluid surrounding the structure is also assumed to have the same cyclic symmetry while the external forces applied on the structure can vary arbitrarily from one sector to another sector.

The physical displacement at the instant t of a point M of the structure with cylindrical coordinates (r, θ, z) can be written as, by using a Fourier decomposition:

$$u(r,\theta,z,t) = \Re\mathrm{e}\left\{\sum_{p=-\infty}^{+\infty} u_p(r,z,t)\mathrm{e}^{\mathrm{i}p\theta}\right\}, \tag{1}$$

where $\Re\mathrm{e}(z)$ is the real part of z and $\mathrm{i}^2 = -1$. By regrouping the terms, we obtain:

$$u(r,\theta,z,t) = \Re\mathrm{e}\left\{\sum_{n=0}^{N-1}\sum_{q=-\infty}^{+\infty} u_{qN+n}(r,z,t)\mathrm{e}^{\mathrm{i}(qN+n)\theta}\right\} = \Re\mathrm{e}\left\{\sum_{n=0}^{N-1} u_n(r,\theta,z,t)\right\}, \tag{2}$$

where $u_n(r,\theta,z,t) = \sum_{q=-\infty}^{+\infty} u_{qN+n}(r,z,t)\mathrm{e}^{\mathrm{i}(qN+n)\theta}$ is the complex travelling wave coordinate corresponding to the phase number n, for $n = 0, \ldots, N-1$.

The travelling wave coordinates u_n of sector S_k, for $k = 0, \ldots, N-1$, are connected to those of the reference sector S_0 by the cyclic symmetry equation:

$$u_n(r,\theta + k\beta, z, t) = u_n(r,\theta,z,t)\mathrm{e}^{\mathrm{i}k\sigma_n}, \tag{3}$$

where $\sigma_n = n\beta$ is the phase angle corresponding to the phase number n.

From Eq. (3), the travelling wave coordinates of the left and the right frontiers of any sector satisfy then the cyclic symmetry boundary condition:

$$u_{n|L_l} = u_{n|L_r}\mathrm{e}^{\mathrm{i}\sigma_n}. \tag{4}$$

Using the cyclic symmetry properties Eq. (3), the motion equation of the structure comes down to N motion equations of the reference sector S_0, in terms of the travelling wave coordinates u_n and with the appropriate second members and boundary conditions. Only sector S_0 has then to be modelized and, after a finite element discretization, the following reduced matrix systems will be solved to obtain the vector of the travelling wave coordinates $\mathbf{u}_n = \mathbf{u}_n(S_0, t)$ of sector S_0, for each phase number $n = 0, \ldots, N-1$:

$$\mathbf{K}\mathbf{u}_n + \mathbf{C}\dot{\mathbf{u}}_n + \mathbf{M}\ddot{\mathbf{u}}_n = \mathbf{f}_{an}(\mathbf{u}_n, \dot{\mathbf{u}}_n) + \mathbf{f}_n + \mathbf{r}_n, \tag{5}$$

$$\mathbf{f}_{an} = \frac{1}{N}\sum_{k=0}^{N-1} \mathbf{f}_a(S_k)\mathrm{e}^{-\mathrm{i}k\sigma_n} \quad \text{and} \quad \mathbf{f}_n = \frac{1}{N}\sum_{k=0}^{N-1} \mathbf{f}(S_k)\mathrm{e}^{-\mathrm{i}k\sigma_n}, \tag{6}$$

$$\mathbf{u}_{n|L_l} = \mathbf{u}_{n|L_r}\mathrm{e}^{\mathrm{i}\sigma_n}. \tag{7}$$

$\mathbf{K}$ is the stiffness matrix of sector S_0, including the centrifugal stress stiffening and the spin softening effects, $\mathbf{C}$ is the damping and gyroscopic effect matrix and $\mathbf{M}$ is the mass matrix. $\mathbf{f}_a(S_k)$ is the vector of the aerodynamic forces applied to sector S_k and which depends on the displacements and the velocities of sector S_k. $\mathbf{f}(S_k)$ is the vector of the other external forces applied to sector S_k, including the centrifugal forces. $\mathbf{r}_n$ is the vector of the interface reactions applied to the frontiers of S_0 with the adjacent sectors, it does not intervene in the solutions of Eqs. (5)–(7) and it is only present due to the constraints Eq. (7). The cyclic symmetry boundary conditions Eq. (7) are expressed in the cylindrical coordinate system.

The vector of the real, physical displacements of sector S_k are obtained from the travelling wave coordinates $\mathbf{u}_n$ by using Eqs. (2) and (3):

$$\mathbf{u}(S_k, t) = \Re\mathrm{e}\left\{\sum_{n=0}^{N-1} \mathbf{u}_n\mathrm{e}^{\mathrm{i}k\sigma_n}\right\}. \tag{8}$$

It is remarked that, since the travelling wave coordinates $\mathbf{u}_m$ satisfy Eq. (3) with the phase angle $\sigma_m = m\beta$ and the fluid is assumed to have the same cyclic symmetry, the physical aerodynamic forces $\mathbf{f}_a(S_k, \mathbf{u}_m, \dot{\mathbf{u}}_m)$ induced by $\mathbf{u}_m$ on sector S_k satisfy:

$$\mathbf{f}_a(S_k, \mathbf{u}_m, \dot{\mathbf{u}}_m) = \mathbf{f}_a(S_0, \mathbf{u}_m, \dot{\mathbf{u}}_m)\mathrm{e}^{\mathrm{i}k\sigma_m}. \tag{9}$$

From Eqs. (6) and (9), the aerodynamic forces induced by $\mathbf{u}_m$ on the travelling wave coordinates $\mathbf{u}_n$ of S_0 are then

$$\mathbf{f}_{an}(\mathbf{u}_m, \dot{\mathbf{u}}_m) = \frac{1}{N}\sum_{k=0}^{N-1} \mathbf{f}_a(S_k, \mathbf{u}_m, \dot{\mathbf{u}}_m)\mathrm{e}^{-\mathrm{i}k\sigma_n} = \mathbf{f}_a(S_0, \mathbf{u}_m, \dot{\mathbf{u}}_m)\delta_{mn}, \tag{10}$$

where δ_{mn} is the Kronecker symbol. Thus, the aerodynamic forces $\mathbf{f}_{an}$ applied to the coordinates $\mathbf{u}_n$ in Eq. (5) depend only on $\mathbf{u}_n$ and not on the other travelling wave coordinates, and they are equal to the physical aerodynamic forces $\mathbf{f}_a(S_0, \mathbf{u}_n, \dot{\mathbf{u}}_n)$ induced by $\mathbf{u}_n$ on sector S_0. This property is also valid for any other rotating external force satisfying Eq. (9), and in particular for the case $m = 0$ where the applied external forces are the same on all sectors.

2.2. Eigenfrequencies and modes of the undamped structure in vacuum

The eigenfrequencies and modes of the undamped structure in vacuum are obtained by solving the following complex eigenvalue system, for each phase number $n = 0, \ldots, N-1$:

$$\mathbf{K}\boldsymbol{\Phi}_n - \mathbf{M}\boldsymbol{\Phi}_n\boldsymbol{\Omega}_n^{*2} = \mathbf{R}_{mn}, \tag{11}$$

$$\boldsymbol{\Phi}_{n|L_l} = \boldsymbol{\Phi}_{n|L_r}\mathrm{e}^{\mathrm{i}\sigma_n}, \tag{12}$$

where $\boldsymbol{\Omega}_n^* = \mathrm{diag}(\omega^*_{n,1}, \ldots, \omega^*_{n,m_n})$ and $\boldsymbol{\Phi}_n = [\boldsymbol{\Phi}_{n,1}, \ldots, \boldsymbol{\Phi}_{n,m_n}]$ are the matrices of the m_n real frequencies and complex modes for the phase number n and $\mathbf{R}_{mn}$ are the modal reactions. The eigensystem Eqs. (11) and (12) is real for $n = 0$ or $n = N/2$ (if N is even), otherwise it is complex and the solutions corresponding to the phase numbers n and $N-n$ are complex conjugate. By convention, we will denote by $-n$ the phase number $N-n$ for $0<n<N/2$. Consequently, we only have to solve Eqs. (11) and (12) for $N/2+1$ or $(N+1)/2$ values of n, depending upon whether N is even or odd. The structure has double modes since the frequencies corresponding to the complex conjugate modes for the phase numbers n and $-n$ are the same:

$$\boldsymbol{\Omega}_{-n} = \boldsymbol{\Omega}_n \quad \text{and} \quad \boldsymbol{\Phi}_{-n} = \overline{\boldsymbol{\Phi}_n} \quad \text{for } 0<n<N/2. \tag{13}$$

The real, physical eigenmodes $\boldsymbol{\Phi}_n^1$ of the structure on sector S_k are obtained by keeping only the modes $\boldsymbol{\Phi}_n$ and $\boldsymbol{\Phi}_{-n}$ in Eq. (8):

$$\boldsymbol{\Phi}_n^1(S_k) = \Re\mathrm{e}(\boldsymbol{\Phi}_n\mathrm{e}^{\mathrm{i}k\sigma_n} + \boldsymbol{\Phi}_{-n}\mathrm{e}^{\mathrm{i}k\sigma_{-n}}) = 2[\Re\mathrm{e}(\boldsymbol{\Phi}_n)\cos k\sigma_n - \Im\mathrm{m}(\boldsymbol{\Phi}_n)\sin k\sigma_n], \tag{14}$$

where $\Im\mathrm{m}(z)$ is the imaginary part of z. For $0<n<N/2$, if the complex eigenmodes $\boldsymbol{\Phi}_n$ are normalized so that ${}^t\overline{\boldsymbol{\Phi}_n}\mathbf{M}\boldsymbol{\Phi}_n = \mathbf{I}$, then $z\boldsymbol{\Phi}_n$ are also eigenmodes with the same norm for any complex number z satisfying $|z| = 1$. By choosing for example $z = \mathrm{i}$, the second real, physical eigenmodes $\boldsymbol{\Phi}_n^2(S_k)$ associated with the double frequencies are obtained by replacing $\boldsymbol{\Phi}_n$ by $\mathrm{i}\boldsymbol{\Phi}_n$ in Eq. (14) and they are deduced from $\boldsymbol{\Phi}_n^1$ by a rotation of angle $\pi/(2\,n)$. For $n = 0$ and $n = N/2$, the frequencies are distinct and $\boldsymbol{\Phi}_n$ are real, thus: $\boldsymbol{\Phi}_n^1(S_k) = \boldsymbol{\Phi}_n^2(S_k) = 2\boldsymbol{\Phi}_n\cos k\sigma_n$.

3. Reduced coupled system

3.1. Modal projection for stability analysis and forced response

For each phase number n, the travelling wave coordinates are expressed as a linear combination of the complex modes:

$$\mathbf{u}_n = \boldsymbol{\Phi}_n\boldsymbol{q}_n, \tag{15}$$

where $\mathbf{q}_n(t)$ is the vector of the m_n complex modal coordinates.

Introducing Eq. (15) in the equation of motion (5) and premultiplying by ${}^t\overline{\boldsymbol{\Phi}_n}$, we obtain the reduced coupled system:

$$\mathbf{K}_{gn}\mathbf{q}_n + \mathbf{C}_{gn}\dot{\mathbf{q}}_n + \mathbf{M}_{gn}\ddot{\mathbf{q}}_n = \mathbf{f}_{agn}(\boldsymbol{\Phi}_n\mathbf{q}_n, \boldsymbol{\Phi}_n\,\dot{\mathbf{q}}_n) + \mathbf{f}_{gn}, \tag{16}$$

with $\mathbf{K}_{gn} = {}^t\overline{\boldsymbol{\Phi}_n}\mathbf{K}\boldsymbol{\Phi}_n$, $\mathbf{C}_{gn} = {}^t\overline{\boldsymbol{\Phi}_n}\mathbf{C}\boldsymbol{\Phi}_n$, $\mathbf{M}_{gn} = {}^t\overline{\boldsymbol{\Phi}_n}\mathbf{M}\boldsymbol{\Phi}_n$, $\mathbf{f}_{agn} = {}^t\overline{\boldsymbol{\Phi}_n}\mathbf{f}_{an}$ and $\mathbf{f}_{gn} = {}^t\overline{\boldsymbol{\Phi}_n}\mathbf{f}_n$; $\mathbf{K}_{gn}$ and $\mathbf{M}_{gn}$ are the diagonal, real generalized stiffness and mass matrices, $\mathbf{C}_{gn}$ is the complex generalized damping and gyroscopic effect matrix, $\mathbf{f}_{agn}$ and $\mathbf{f}_{gn}$ are the complex generalized aerodynamic and external forces. As the modes $\boldsymbol{\Phi}_n$ have already satisfied the cyclic symmetry boundary conditions Eq. (7), the latter are already taken into account and by consequent the interface reactions disappear from Eq. (16). In general, Eq. (16) should be solved for each phase number $n = 0, \ldots, N-1$ as we no longer have $\mathbf{u}_{-n} = \bar{\mathbf{u}}_n$ for $0<n<N/2$, except when $\mathbf{C} = \mathbf{0}$.

For the aeroelastic stability analysis, all the external forces are null except the aerodynamic forces. The solutions are looked up under the form:

$$\mathbf{u}_n(t) = \tilde{\mathbf{u}}_n\, \mathrm{e}^{pt} \quad \text{and} \quad \mathbf{q}_n(t) = \tilde{\mathbf{q}}_n \mathrm{e}^{pt} \quad \text{with } p = \mathrm{i}\omega(1 + \mathrm{i}\alpha), \tag{17}$$

where ω is the unknown aeroelastic eigenfrequency ($\omega > 0$) and α is the unknown aeroelastic damping factor ($\alpha \in \mathbb{R}$). Using the hypothesis of linearity, the aerodynamic forces become:

$$\mathbf{f}_{an}(\boldsymbol{\Phi}_n\mathbf{q}_n, \boldsymbol{\Phi}_n\, \dot{\mathbf{q}}_n) = \mathbf{F}_{an}(\boldsymbol{\Phi}_n\, \mathrm{e}^{pt}, \boldsymbol{\Phi}_n p \mathrm{e}^{pt})\tilde{\mathbf{q}}_n = \tilde{\mathbf{F}}_{an}(\boldsymbol{\Phi}_n, p)\tilde{\mathbf{q}}_n \mathrm{e}^{pt}, \tag{18}$$

where $\mathbf{F}_{an}(\boldsymbol{\Phi}_n \mathrm{e}^{pt}, \boldsymbol{\Phi}_n p \mathrm{e}^{pt})$ is the matrix whose ith column is the aerodynamic force induced by the displacement $\boldsymbol{\Phi}_{n,i}\mathrm{e}^{pt}$. The generalized aerodynamic forces are written in the form:

$$\mathbf{f}_{agn}(\boldsymbol{\Phi}_n\mathbf{q}_n, \boldsymbol{\Phi}_n\dot{\mathbf{q}}_n) = {}^{\mathrm{t}}\overline{\boldsymbol{\Phi}_n}\tilde{\mathbf{F}}_{an}(\boldsymbol{\Phi}_n, p)\tilde{\mathbf{q}}_n \mathrm{e}^{pt} = \tilde{\mathbf{F}}_{agn}(\boldsymbol{\Phi}_n, p)\tilde{\mathbf{q}}_n \mathrm{e}^{pt}. \tag{19}$$

Substituting Eqs. (17) and (19) in Eq. (16), we obtain the flutter equation:

$$[\mathbf{K}_{gn} + p\mathbf{C}_{gn} + p^2\mathbf{M}_{gn} - \tilde{\mathbf{F}}_{agn}(\boldsymbol{\Phi}_n, p)]\tilde{\mathbf{q}}_n = \mathbf{0}, \tag{20}$$

which is a complex, nonlinear eigenvalue system in which the aerodynamic coefficient matrix $\tilde{\mathbf{F}}_{agn}(\boldsymbol{\Phi}_n, p)$ depends on the complex modes $\boldsymbol{\Phi}_n$ and the unknown complex eigenvalue p. An approximated expression of $\tilde{\mathbf{F}}_{agn}(\boldsymbol{\Phi}_n, p)$ in terms of p can be obtained by Karpel's minimum state smoothing method from the tabulated values of $\tilde{\mathbf{F}}_{agn}(\boldsymbol{\Phi}_n, p)$ computed at discrete frequencies, i.e. for $p = \mathrm{i}\omega_1, \ldots, \mathrm{i}\omega_{n_\omega}$.

For the frequency response to a harmonic external force $\mathbf{f}_n(t) = \tilde{\mathbf{f}}_n \mathrm{e}^{\mathrm{i}\omega t}$ where ω is a given excitation frequency, the solution is looked up under the form $\mathbf{u}_n(t) = \tilde{\mathbf{u}}_n \mathrm{e}^{\mathrm{i}\omega t}$ and $\mathbf{q}_n(t) = \tilde{\mathbf{q}}_n \mathrm{e}^{\mathrm{i}\omega t}$. Substituting Eqs. (17)–(19) in Eq. (16) with $p = \mathrm{i}\omega$, we obtain a linear system for the frequency response $\tilde{\mathbf{q}}_n(\omega)$ in which the aerodynamic coefficient matrix $\tilde{\mathbf{F}}_{agn}(\boldsymbol{\Phi}_n, \mathrm{i}\omega)$ is perfectly determined:

$$[\mathbf{K}_{gn} + \mathrm{i}\omega\mathbf{C}_{gn} - \omega^2\mathbf{M}_{gn} - \tilde{\mathbf{F}}_{agn}(\boldsymbol{\Phi}_n, \mathrm{i}\omega)]\tilde{\mathbf{q}}_n = \tilde{\mathbf{f}}_{gn}. \tag{21}$$

For the time response, Karpel's minimum state approximation is used to obtain a time-domain expression of the generalized aerodynamic forces from the tabulated aerodynamic coefficient matrices:

$$\mathbf{f}_{agn}(\boldsymbol{\Phi}_n\mathbf{q}_n, \boldsymbol{\Phi}_n\dot{\mathbf{q}}_n) = \mathbf{f}_{agn}(\boldsymbol{\Phi}_n, \mathbf{q}_n, \dot{\mathbf{q}}_n, \ddot{\mathbf{q}}_n, \mathbf{z}_n), \tag{22}$$

where $\mathbf{z}_n$ are the auxiliary state variables. The time integration is then performed simultaneously on the reduced coupled system Eq. (16) and the differential equations introduced by the auxiliary variables.

3.2. The Craig and Bampton projection basis

In order to take into account structural nonlinearities such as friction or free-play in the reduced coupled system Eq. (16), we need to keep some physical coordinates among the generalized coordinates $\mathbf{q}_n$. These "nonlinear" coordinates $\mathbf{u}_{n|NL}$ can be for example the displacements of the reference sector nodes located at the junction between the blade and the disk, where friction dampers are introduced. For this aim, the Craig and Bampton (1968) projection basis is used instead of the eigenmodes of the structure. It is composed of two sets of vectors:

(i) the first m_n complex eigenmodes $\boldsymbol{\Phi}_n$ of the undamped reference sector in vacuum, obtained by applying the cyclic symmetry boundary conditions Eq. (7) and by holding $\mathbf{u}_{n|NL}$ fixed:

$$\mathbf{K}\boldsymbol{\Phi}_n - \mathbf{M}\boldsymbol{\Phi}_n\boldsymbol{\Omega}_n^{*2} = \mathbf{R}_{mn} \quad \text{with } \boldsymbol{\Phi}_{n|L_l} = \boldsymbol{\Phi}_{n|L_r}\mathrm{e}^{\mathrm{i}\sigma_n} \quad \text{and} \quad \boldsymbol{\Phi}_n|_{NL} = \mathbf{0}; \tag{23}$$

(ii) the constraint modes $\boldsymbol{\Psi}_{cn}$ which are the complex static solutions of the reference sector obtained by applying the cyclic symmetry boundary conditions Eq. (7) and by imposing successively a unit displacement on one coordinate of $\mathbf{u}_{n|NL}$, while holding the remaining coordinates of $\mathbf{u}_{n|NL}$ fixed:

$$\mathbf{K}\boldsymbol{\Psi}_{cn} = \mathbf{R}_{cn} \quad \text{with } \boldsymbol{\Psi}_{cn|L_l} = \boldsymbol{\Psi}_{cn|L_r}\mathrm{e}^{\mathrm{i}\sigma_n} \quad \text{and} \quad \boldsymbol{\Psi}_{cn|NL} = \mathbf{I}. \tag{24}$$

The travelling wave coordinates of the reference sector are then expressed as a linear combination of the vectors of the Craig and Bampton basis:

$$\mathbf{u}_n = \boldsymbol{\Phi}_n\boldsymbol{\eta}_n + \boldsymbol{\Psi}_{cn}\mathbf{u}_{n|NL} = \mathbf{Q}_n\mathbf{q}_n, \tag{25}$$

with $\mathbf{Q}_n = [\boldsymbol{\Phi}_n, \boldsymbol{\Psi}_{cn}]$, $\mathbf{q}_n = {}^{\mathrm{t}}[{}^{\mathrm{t}}\boldsymbol{\eta}_n, {}^{\mathrm{t}}\mathbf{u}_{n|NL}]$ and $\boldsymbol{\eta}_n$ is the vector of the modal generalized coordinates.

Introducing Eq. (25) in the equation of motion Eq. (5) and premultiplying by ${}^{\mathrm{t}}\overline{\mathbf{Q}_n}$, we obtain a complex reduced coupled system similar to Eq. (16):

$$\mathbf{K}_{rn}\mathbf{q}_n + \mathbf{C}_{rn}\dot{\mathbf{q}}_n + \mathbf{M}_{rn}\ddot{\mathbf{q}}_n = \mathbf{f}_{agn}(\mathbf{Q}_n\mathbf{q}_n, \mathbf{Q}_n\dot{\mathbf{q}}_n) + \mathbf{f}_{gn}, \tag{26}$$

where $\mathbf{K}_{rn} = {}^t\overline{\mathbf{Q}_n}\mathbf{K}\mathbf{Q}_n$, $\mathbf{C}_{rn} = {}^t\overline{\mathbf{Q}_n}\mathbf{C}\mathbf{Q}_n$ and $\mathbf{M}_{rn} = {}^t\overline{\mathbf{Q}_n}\mathbf{M}\mathbf{Q}_n$ are the complex reduced stiffness, damping and mass matrices and $\mathbf{f}_{agn} = {}^t\overline{\mathbf{Q}_n}\mathbf{f}_{an}$ and $\mathbf{f}_{gn} = {}^t\overline{\mathbf{Q}_n}\mathbf{f}_n$ are the complex generalized unsteady aerodynamic and external forces. As in Eq. (16), the cyclic symmetry boundary conditions are already taken into account in the Craig and Bampton basis, so the interface reactions disappear in Eq. (26). The size of the reduced system Eq. (26) is the number of eigenmodes plus the number of the nonlinear coordinates.

4. Computation of the generalized aerodynamic forces

4.1. Generalized aerodynamic forces

The unsteady aerodynamic forces are computed from a basis of m_n real mode shapes $\mathbf{\Psi}$ of the reference sector, for an oscillation frequency ω and an inter-blade phase angle σ_n. By expressing the displacements of the reference sector as a linear combination of the modes $\mathbf{\Psi}$ and by assuming that the structural motion is harmonic and that all the sectors have the same motion with a constant phase angle σ_n between two adjacent sectors, i.e.,

$$\mathbf{u}_n(t) = \mathbf{u}_n(S_0, t) = \mathbf{\Psi}\tilde{\mathbf{q}}_n e^{i\omega t} \quad \text{and} \quad \mathbf{u}_n(S_k, t) = \mathbf{\Psi}\tilde{\mathbf{q}}_n e^{i\omega t} e^{ik\sigma_n}, \tag{27}$$

the generalized aerodynamic forces generated by the displacement $\mathbf{u}_n(t)$ are written, by linearity, as

$$\mathbf{f}_{agn}(\mathbf{u}_n(t), \dot{\mathbf{u}}_n(t)) = {}^t\mathbf{\Psi}\mathbf{F}_{an}(\mathbf{\Psi}, i\omega, t)\tilde{\mathbf{q}}_n = \mathbf{F}_{agn}(\mathbf{\Psi}, i\omega, t)\tilde{\mathbf{q}}_n. \tag{28}$$

$\mathbf{F}_{an}(\mathbf{\Psi}, i\omega, t)$ is the matrix whose jth column is the unsteady aerodynamic force $\mathbf{f}_{an}(\mathbf{\Psi}_j, i\omega, t)$ generated by the harmonic motion of the jth mode and $\mathbf{F}_{agn}(\mathbf{\Psi}, i\omega, t) = {}^t\mathbf{\Psi}\mathbf{F}_{an}(\mathbf{\Psi}, i\omega, t)$ is the time-dependant aerodynamic coefficient matrix.

The unsteady aerodynamic force generated at a point M of the surface Σ of the structure by the harmonic motion of the jth mode is given by

$$\vec{f_{an}}(M, \mathbf{\Psi}_j, i\omega, t) = -[P_n(M, \mathbf{\Psi}_j, i\omega, t) - P_s(M)]\,\vec{n}(M)\, d\Sigma \quad \text{for } M \in \Sigma, \tag{29}$$

where P_n is the unsteady pressure, P_s the steady pressure, $\vec{n}$ is the unit external normal vector to the surface Σ and $d\Sigma$ is an elementary surface of Σ. Taking the scalar product of this unsteady aerodynamic force and the displacement vector $\vec{\Psi}_i(M)$ of the ith mode at the point M and integrating over the surface Σ, we obtain the (i,j)-term of the aerodynamic coefficient matrix $\mathbf{F}_{agn}(\mathbf{\Psi}, i\omega, t)$:

$${}^t\mathbf{\Psi}_i\mathbf{f}_{an}(\mathbf{\Psi}_j, i\omega, t) = -\int_{M\in\Sigma}[P_n(M, \mathbf{\Psi}_j, i\omega, t) - P_s(M)]\,\vec{n}(M)\cdot\vec{\Psi}_i(M)\, d\Sigma. \tag{30}$$

We introduce the aerodynamic coefficient matrix $\mathbf{A}_n(\mathbf{\Psi}, i\omega, t)$ obtained from the integral in Eq. (30) with P_n and P_s replaced by the associated pressure coefficient $C_P = (P - P_\infty)/(\frac{1}{2}\rho_\infty V_\infty^2)$, where P_∞, ρ_∞ and V_∞ are the pressure, the density and the velocity of the upstream unperturbed fluid. By performing a Fourier analysis of $\mathbf{F}_{agn}(\mathbf{\Psi}, i\omega, t)$ and by keeping only the first harmonic term, we have:

$$\mathbf{F}_{agn}(\mathbf{\Psi}, i\omega, t) \simeq \tilde{\mathbf{F}}_{agn}(\mathbf{\Psi}, i\omega)e^{i\omega t} = -\tfrac{1}{2}\rho_\infty V_\infty^2 \tilde{\mathbf{A}}_n(\mathbf{\Psi}, i\omega)e^{i\omega t}. \tag{31}$$

The generalized aerodynamic forces generated by the displacement $\mathbf{u}_n(t)$ become:

$$\mathbf{f}_{agn}(\mathbf{u}_n(t), \dot{\mathbf{u}}_n(t)) \simeq \tilde{\mathbf{F}}_{agn}(\mathbf{\Psi}, i\omega)\tilde{\mathbf{q}}_n e^{i\omega t} = -\tfrac{1}{2}\rho_\infty V_\infty^2 \tilde{\mathbf{A}}_n(\mathbf{\Psi}, i\omega)\tilde{\mathbf{q}}_n e^{i\omega t}. \tag{32}$$

$\tilde{\mathbf{F}}_{agn}(\mathbf{\Psi}, i\omega)$ and $\tilde{\mathbf{A}}_n(\mathbf{\Psi}, i\omega)$ are complex, asymmetric square matrices of dimension m_n. In practice, they are computed for n_ω oscillation frequencies $\omega_1, \ldots, \omega_{n_\omega}$.

4.2. Aerodynamic coefficient matrix for complex modes

In the previous section, the aerodynamic coefficient matrices $\tilde{\mathbf{F}}_{agn}(\mathbf{\Psi}, i\omega)$ and $\tilde{\mathbf{A}}_n(\mathbf{\Psi}, i\omega)$ were computed from a basis of real mode shapes $\mathbf{\Psi}$. In the flutter equation (20), the aerodynamic coefficient matrix should be determined from the m_n complex modes $\mathbf{\Phi}_n$, for $0<n<N/2$. Denoting by $\mathbf{\Phi}_n'$ and $\mathbf{\Phi}_n''$ the real and imaginary parts of $\mathbf{\Phi}_n$, the aerodynamic coefficient matrix $\tilde{\mathbf{F}}_{agn}(\mathbf{\Phi}_n, i\omega)$ generated by the complex modes $\mathbf{\Phi}_n$ is written as, using the linearity hypothesis:

$$\tilde{\mathbf{F}}_{agn}(\mathbf{\Phi}_n, i\omega) = {}^t\overline{\mathbf{\Phi}_n}\tilde{\mathbf{F}}_{an}(\mathbf{\Phi}_n, i\omega) = [{}^t\mathbf{\Phi}_n' - i\,{}^t\mathbf{\Phi}_n''][\tilde{\mathbf{F}}_{an}(\mathbf{\Phi}_n', i\omega) + i\tilde{\mathbf{F}}_{an}(\mathbf{\Phi}_n'', i\omega)]. \tag{33}$$

The matrices which compose $\tilde{\mathbf{F}}_{agn}(\mathbf{\Phi}_n, \mathrm{i}\omega)$ can be extracted from the aerodynamic coefficient matrix obtained by using the basis of the $2m_n$ real vectors formed by $\mathbf{\Phi}'_n$ and $\mathbf{\Phi}''_n$. We indeed have

$$\tilde{\mathbf{F}}_{agn}([\mathbf{\Phi}'_n, \mathbf{\Phi}''_n], \mathrm{i}\omega) = \begin{bmatrix} {}^{\mathrm{t}}\mathbf{\Phi}'_n \tilde{\mathbf{F}}_{an}(\mathbf{\Phi}'_n, \mathrm{i}\omega) & {}^{\mathrm{t}}\mathbf{\Phi}'_n \tilde{\mathbf{F}}_{an}(\mathbf{\Phi}''_n, \mathrm{i}\omega) \\ {}^{\mathrm{t}}\mathbf{\Phi}''_n \tilde{\mathbf{F}}_{an}(\mathbf{\Phi}'_n, \mathrm{i}\omega) & {}^{\mathrm{t}}\mathbf{\Phi}''_n \tilde{\mathbf{F}}_{an}(\mathbf{\Phi}''_n, \mathrm{i}\omega) \end{bmatrix}. \tag{34}$$

4.3. Aerodynamic computations

The unsteady aerodynamic forces are obtained solving the Euler equations for an ideal gas using an aerodynamic code called CANARI and developed for years at ONERA (Dugeai et al., 2000). This code is based on the finite volume method. The time integration is performed using a 3-D cell-centered Jameson-like four stages Runge–Kutta scheme (Jameson et al., 1981). Second- and fourth-order artificial viscosity terms are added to improve the stability when strong nonlinearities like shocks occur. Because of the cyclic symmetry of the flow, a chorochronic boundary condition is applied to the simulated channel. This condition reads:

$$F(r, \theta + k\beta, z, t) = F\left(r, \theta, z, t + \frac{k\sigma_n}{\omega}\right) \quad \text{for } n = 0, \ldots, N-1 \text{ and } \forall k \in \mathbb{N}, \tag{35}$$

where F is any flowfield variable, r is the rotation radius, and θ the azimuthal angle. The following condition is applied at the outflow:

$$\frac{\partial P}{\partial r} = \rho \frac{V^2_{\mathrm{abs,tang}}}{r} \tag{36}$$

where P is the pressure, ρ is the density, and $V_{\mathrm{abs,tang}}$ is the tangent component of the velocity expressed in a nonrotating frame of reference.

In a first step, a steady state is computed depending on the rotation speed, on the pressure ratio and on the far-field total temperature, total pressure, and velocity. In a second step, unsteady simulations are performed by forcing an oscillating blade motion at different frequencies. These simulations depend on the steady flowfield previously computed and used as initial conditions, on the inter-blade phase angle, and on the forced motion shape and frequency. A blowing condition is then used to simulate the blade motion. Once a pseudo-steady oscillating state has been reached (no transient effect), a Fourier transform is performed over the pressure to get the unsteady aerodynamic forces.

5. Solution of the coupled system

5.1. Double scanning method

The flutter equation (20) is written using the aerodynamic coefficient matrix $\tilde{\mathbf{A}}_n(\mathbf{\Phi}_n, p)$ defined in Eq. (32):

$$[\mathbf{K}_{gn} + p\mathbf{C}_{gn} + p^2\mathbf{M}_{gn} + \tfrac{1}{2}\rho_\infty V_\infty^2 \tilde{\mathbf{A}}_n(\mathbf{\Phi}_n, p)]\tilde{\mathbf{q}}_n = \mathbf{0}. \tag{37}$$

For motions defined by Eq. (17) in the frequency domain, $\tilde{\mathbf{A}}_n(\mathbf{\Phi}_n, p)$ depends only on the quotient pc/V_∞ and can be written as

$$\tilde{\mathbf{A}}_n(\mathbf{\Phi}_n, p) = \tilde{\mathbf{A}}_n(\mathbf{\Phi}_n, pc/V_\infty) = \tilde{\mathbf{A}}'_n(\mathbf{\Phi}_n, pc/V_\infty) + \mathrm{i}\tilde{\mathbf{A}}''_n(\mathbf{\Phi}_n, pc/V_\infty), \tag{38}$$

where c is a reference length, for example the blade chord, $\tilde{\mathbf{A}}'_n(\mathbf{\Phi}_n, pc/V_\infty)$ and $\tilde{\mathbf{A}}''_n(\mathbf{\Phi}_n, pc/V_\infty)$ are the real and imaginary parts of $\tilde{\mathbf{A}}_n(\mathbf{\Phi}_n, pc/V_\infty)$. Substituting Eq. (38) into Eq. (37), we obtain

$$[\mathbf{K}^*_{gn}(pc/V_\infty) + p\mathbf{C}^*_{gn}(pc/V_\infty) + p^2\mathbf{M}_{gn}]\tilde{\mathbf{q}}_n = \mathbf{0}, \tag{39}$$

with

$$\mathbf{K}^*_{gn}(pc/V_\infty) = \mathbf{K}_{gn} + \tfrac{1}{2}\rho_\infty V_\infty^2 \tilde{\mathbf{A}}'_n(\mathbf{\Phi}_n, pc/V_\infty),$$

$$\mathbf{C}^*_{gn}(pc/V_\infty) = \mathbf{C}_{gn} + \mathrm{i}\tfrac{1}{2}c\rho_\infty V_\infty \frac{\tilde{\mathbf{A}}''_n(\mathbf{\Phi}_n, pc/V_\infty)}{pc/V_\infty}.$$

Let us consider the reduced frequency

$$\kappa = \omega c / V_\infty. \tag{40}$$

For a small damping factor, $|\alpha| \ll 1$, the following approximations can be made:

$$\tilde{\mathbf{A}}_n(\mathbf{\Phi}_n, pc/V_\infty) \simeq \tilde{\mathbf{A}}_n(\mathbf{\Phi}_n, \mathrm{i}\kappa) = \tilde{\mathbf{A}}_n'(\mathbf{\Phi}_n, \mathrm{i}\kappa) + \mathrm{i}\tilde{\mathbf{A}}_n''(\mathbf{\Phi}_n, \mathrm{i}\kappa), \tag{41}$$

$$\mathbf{K}^*_{gn}(pc/V_\infty) \simeq \mathbf{K}^*_{gn}(\mathrm{i}\kappa) = \mathbf{K}_{gn} + \tfrac{1}{2}\rho_\infty V_\infty^2 \tilde{\mathbf{A}}_n'(\mathbf{\Phi}_n, \mathrm{i}\kappa), \tag{42}$$

$$\mathbf{C}^*_{gn}(pc/V_\infty) \simeq \mathbf{C}^*_{gn}(\mathrm{i}\kappa) = \mathbf{C}_{gn} + \tfrac{1}{2}c\rho_\infty V_\infty \tilde{\mathbf{A}}_n''(\mathbf{\Phi}_n, \mathrm{i}\kappa)/\kappa. \tag{43}$$

Substituting Eqs. (42) and (43) in Eq. (39), we obtain an approximate flutter equation:

$$[\mathbf{K}^*_{gn}(\mathrm{i}\kappa) + p\mathbf{C}^*_{gn}(\mathrm{i}\kappa) + p^2\mathbf{M}_{gn}]\tilde{\mathbf{q}}_n = \mathbf{0} \quad \text{with } \kappa = \Im\mathrm{m}(p)c/V_\infty, \tag{44}$$

which can be written under the form of a nonlinear eigenvalue system of dimension $2m_n$:

$$\begin{bmatrix} \mathbf{0} & \mathbf{I} \\ -\mathbf{M}_{gn}^{-1}\mathbf{K}^*_{gn}(\mathrm{i}\kappa) & -\mathbf{M}_{gn}^{-1}\mathbf{C}^*_{gn}(\mathrm{i}\kappa) \end{bmatrix} \begin{Bmatrix} \tilde{\mathbf{q}}_n \\ p\tilde{\mathbf{q}}_n \end{Bmatrix} = p \begin{Bmatrix} \tilde{\mathbf{q}}_n \\ p\tilde{\mathbf{q}}_n \end{Bmatrix}, \tag{45}$$

or

$$\mathbf{H}(\mathrm{i}\kappa)\mathbf{x} = p\mathbf{x} \quad \text{with } \kappa = \Im\mathrm{m}(p)c/V_\infty. \tag{46}$$

The matrices $\mathbf{K}^*_{gn}(\mathrm{i}\kappa)$, $\mathbf{C}^*_{gn}(\mathrm{i}\kappa)$ and $\mathbf{H}(\mathrm{i}\kappa)$ are real and depend on $\tilde{\mathbf{A}}_n'(\mathbf{\Phi}_n, \mathrm{i}\kappa)$, $\tilde{\mathbf{A}}_n''(\mathbf{\Phi}_n, \mathrm{i}\kappa)$ and the upstream infinite velocity V_∞. The aerodynamic coefficient matrices $\tilde{\mathbf{A}}_n'(\mathbf{\Phi}_n, \mathrm{i}\kappa)$ and $\tilde{\mathbf{A}}_n''(\mathbf{\Phi}_n, \mathrm{i}\kappa)$ have been tabulated for n_κ increasing reduced frequencies $\kappa_1, \ldots, \kappa_{n_\kappa}$. The eigensolutions $(p, \mathbf{x})$ of Eq. (45) are computed for n_V increasing velocities $V_\infty^1, \ldots, V_\infty^{n_V}$ and should satisfy $\omega = \Im\mathrm{m}(p) = \kappa V_\infty / c$. For each velocity V_∞^k, the following eigensystems are solved, for $i = 1, \ldots, 2m_n$ and $j = 0, 1, 2, \ldots$, until the convergence on κ is obtained:

$$\mathbf{H}(\mathrm{i}\kappa_{i,j})\mathbf{x}_{i,j+1} = p_{i,j+1}\mathbf{x}_{i,j+1} \quad \text{with } \kappa_{i,j} = \omega_{i,j}c/V_\infty^k = \Im\mathrm{m}(p_{i,j})c/V_\infty^k, \tag{47}$$

where $(p_{i,j}, \mathbf{x}_{i,j})$ is the ith eigensolution obtained at the jth iteration. The matrix $\mathbf{H}(\mathrm{i}\kappa_{i,j})$ is computed by interpolating $\tilde{\mathbf{A}}_n'(\mathbf{\Phi}_n, \mathrm{i}\kappa)$ and $\tilde{\mathbf{A}}_n''(\mathbf{\Phi}_n, \mathrm{i}\kappa)/\kappa$ from the tabulated values. The starting frequencies $\omega_{i,0}$ are obtained by extrapolating the frequencies at V_∞^{k-1} and V_∞^{k-2} if $k > 2$. For the second velocity V_∞^2, $\omega_{i,0}$ are the frequencies obtained at V_∞^1 and for the first velocity V_∞^1, $\omega_{i,0}$ are the frequencies of the structure in vacuum.

This iterative process amounts to performing a double scanning, the first one on V_∞ and the second one on κ, and to finding out, for each velocity V_∞^k, the intersections between the straight line $\omega = (V_\infty^k/c)\kappa$ and the evolution curves of the frequencies in function of κ, $\omega_i = \Im\mathrm{m}(p_i(\kappa))$, obtained by interpolating the imaginary parts of the eigenvalues of $\mathbf{H}(\mathrm{i}\kappa_1), \ldots, \mathbf{H}(\mathrm{i}\kappa_{n_\kappa})$.

This method allows the determination of all the eigenvalues required for the stability analysis. We obtain the evolution of the aeroelastic frequencies and dampings as functions of the velocity or the mass flow of the upstream unperturbed fluid. Flutter occurs if the damping factor α is negative.

It is remarked that the double scanning method is not valid for small velocities since the latter lead to very large reduced frequencies which will be out of the range of the tabulated values, and therefore the extrapolation of the aerodynamic coefficient matrix from the tabulated ones in the iterative solution of Eq. (46) will give incorrect results.

5.2. Minimum state smoothing method

The aerodynamic coefficient matrix $\tilde{\mathbf{A}}_n(\mathbf{\Phi}_n, \mathrm{i}\omega)$ has been computed for n_κ reduced frequencies $\kappa_1, \ldots, \kappa_{n_\kappa}$ defined by Eq. (40) with the assumption of harmonic motion. For arbitrary motions like those defined by Eq. (17), it is necessary to extend the values of the aerodynamic coefficient matrix to an area of the complex plane containing the imaginary axis, i.e. to determine $\tilde{\mathbf{A}}_n(\mathbf{\Phi}_n, p)$ for $p = \mathrm{i}\omega(1 + \mathrm{i}\alpha)$ with $\alpha \neq 0$.

The minimum state smoothing method (Karpel, 1982, 1990) consists in modelling the generalized aerodynamic forces by using a rational approximation and auxiliary state variables:

$$\tilde{\mathbf{A}}_n(\mathbf{\Phi}_n, p) \simeq \mathbf{A}_{n0} + \frac{pc}{V_\infty}\mathbf{A}_{n1} + \frac{p^2c^2}{V_\infty^2}\mathbf{A}_{n2} + \frac{pc}{V_\infty}\mathbf{D}_n\left[\frac{pc}{V_\infty}\mathbf{I} - \mathbf{R}_n\right]^{-1}\mathbf{E}_n. \tag{48}$$

The matrices $\mathbf{A}_{n0}$, $\mathbf{A}_{n1}$, $\mathbf{A}_{n2}$, $\mathbf{D}_n$, $\mathbf{R}_n$ and $\mathbf{E}_n$ are real with dimensions $(m_n \times m_n)$ for $\mathbf{A}_{n0}$, $\mathbf{A}_{n1}$ and $\mathbf{A}_{n2}$, $(m_n \times n_p)$ for $\mathbf{D}_n$, $(n_p \times m_n)$ for $\mathbf{E}_n$ and $\mathbf{R}_n = \mathrm{diag}(r_1, \ldots, r_{n_p})$ where n_p is the degree of the denominator of the rational function or the number of poles and $r_i < 0$ are the poles. These matrices are computed by using a method of least squares minimization; see Appendix A and Poirion (1995).

Using Eq. (48), the flutter equation (37) can be written under the form of a nonlinear eigenvalue system of dimension $2m_n$:

$$\begin{bmatrix} \mathbf{0} & \mathbf{I} \\ -\mathbf{M}_{gn}^{*-1}[\mathbf{K}_{gn}^{*} + \mathbf{G}_n(p)] & -\mathbf{M}_{gn}^{*-1}\mathbf{C}_{gn}^{*} \end{bmatrix} \begin{Bmatrix} \tilde{\mathbf{q}}_n \\ p\tilde{\mathbf{q}}_n \end{Bmatrix} = p \begin{Bmatrix} \tilde{\mathbf{q}}_n \\ p\tilde{\mathbf{q}}_n \end{Bmatrix}, \tag{49}$$

or

$$\mathbf{H}(p)\mathbf{x} = p\mathbf{x} \tag{50}$$

with

$$\mathbf{K}_{gn}^{*} = \mathbf{K}_{gn} + \tfrac{1}{2}\rho_\infty V_\infty^2 \mathbf{A}_n^0, \quad \mathbf{C}_{gn}^{*} = \mathbf{C}_{gn} + \tfrac{1}{2}\rho_\infty c V_\infty \mathbf{A}_{n1},$$

$$\mathbf{M}_{gn}^{*} = \mathbf{M}_{gn} + \tfrac{1}{2}\rho_\infty c^2 \mathbf{A}_n^2, \quad \mathbf{G}_n(p) = \tfrac{1}{2}\rho_\infty V_\infty pc\mathbf{D}_n[(pc/V_\infty)\mathbf{I} - \mathbf{R}_n]^{-1}\mathbf{E}_n.$$

The matrices $\mathbf{G}_n(p)$ and $\mathbf{H}(p)$ are complex and depend on V_∞. The eigensolutions $(p, \mathbf{x})$ of Eq. (50) are computed for n_V increasing velocities $V_\infty^1, \ldots, V_\infty^{n_V}$. This nonlinear eigenvalue problem is solved using an iterative process based on the method of successive approximations for finding a fixed point of a function (Appendix B).

To obtain the approximation Eq. (48), n_p auxiliary state variables $\tilde{\mathbf{z}}_n$ have been defined by

$$\tilde{\mathbf{z}}_n = \frac{pc}{V_\infty}\left[\frac{pc}{V_\infty}\mathbf{I} - \mathbf{R}_n\right]^{-1}\mathbf{E}_n\tilde{\mathbf{q}}_n. \tag{51}$$

In the frequency domain, these auxiliary variables satisfy

$$p\tilde{\mathbf{z}}_n = (V_\infty/c)\mathbf{R}_n\tilde{\mathbf{z}}_n + p\mathbf{E}_n\tilde{\mathbf{q}}_n, \tag{52}$$

and they are solutions of a system of first-order differential equations in the time domain:

$$\dot{\mathbf{z}}_n(t) = (V_\infty/c)\mathbf{R}_n\mathbf{z}_n(t) + \mathbf{E}_n\dot{\mathbf{q}}_n(t). \tag{53}$$

The generalized aerodynamic forces are then written in the frequency and time domains as

$$\tilde{\mathbf{F}}_{agn}(\mathbf{\Phi}_n, p)\tilde{\mathbf{q}}_n = -\tfrac{1}{2}\rho_\infty V_\infty^2\left(\mathbf{A}_{n0} + \frac{pc}{V_\infty}\mathbf{A}_{n1} + \frac{p^2c^2}{V_\infty^2}\mathbf{A}_{n2}\right)\tilde{\mathbf{q}}_n - \tfrac{1}{2}\rho_\infty V_\infty^2\mathbf{D}_n\tilde{\mathbf{z}}_n, \tag{54}$$

$$\mathbf{f}_{agn}(\mathbf{\Phi}_n\mathbf{q}_n, \mathbf{\Phi}_n\dot{\mathbf{q}}_n) = -\tfrac{1}{2}\rho_\infty V_\infty^2\left(\mathbf{A}_{n0}\mathbf{q}_n + \frac{c}{V_\infty}\mathbf{A}_{n1}\dot{\mathbf{q}}_n + \frac{c^2}{V_\infty^2}\mathbf{A}_{n2}\ddot{\mathbf{q}}_n + \mathbf{D}_n\mathbf{z}_n\right). \tag{55}$$

Substituting Eq. (55) in the reduced coupled system Eq. (16) and combining with Eq. (53), we obtain a linear system of second-order differential equations of dimension $m_n + n_p$:

$$\begin{bmatrix} \mathbf{K}_{gn}^{*} & \tfrac{1}{2}\rho_\infty V_\infty^2\mathbf{D}_n \\ \mathbf{0} & (V_\infty/c)\mathbf{R}_n \end{bmatrix}\begin{Bmatrix} \mathbf{q}_n \\ \mathbf{z}_n \end{Bmatrix} + \begin{bmatrix} \mathbf{C}_{gn}^{*} & \mathbf{0} \\ \mathbf{E}_n & -\mathbf{I} \end{bmatrix}\begin{Bmatrix} \dot{\mathbf{q}}_n \\ \dot{\mathbf{z}}_n \end{Bmatrix} + \begin{bmatrix} \mathbf{M}_{gn}^{*} & \mathbf{0} \\ \mathbf{0} & \mathbf{0} \end{bmatrix}\begin{Bmatrix} \ddot{\mathbf{q}}_n \\ \ddot{\mathbf{z}}_n \end{Bmatrix} = \begin{Bmatrix} \mathbf{f}_{gn} \\ \mathbf{0} \end{Bmatrix}, \tag{56}$$

where $\mathbf{K}_{gn}^{*}$, $\mathbf{C}_{gn}^{*}$ and $\mathbf{M}_{gn}^{*}$ are the same matrices as in Eq. (49).

The second-order system (56) is solved using the Newmark numerical integration scheme.

6. Numerical applications

The previously described coupling methods have been applied to a numerical model of a compressor disk composed of 22 large chord blades, for different rotation speeds and phase angles.

The structural finite element model of a reference sector with one blade has 19 539 degrees of freedom. The eigenfrequencies and modes in vacuum are computed by using the cyclic symmetry and by taking into account the geometrical stiffness matrix due to the centrifugal stress generated by the rotation.

The aerodynamic computations were performed on a two-block structured grid, each block having $61 \times 18 \times 30$ points with 60 points on the profile. Fig. 1 shows the mesh of one channel of the embedding fluid.

The different coupling methods used for the test cases are summarized in Table 1. In addition to the indirect coupling methods described in this paper and for comparison, we also use the direct coupling method in the time domain where the fluid and the structure motion equations are solved alternately at each time step.

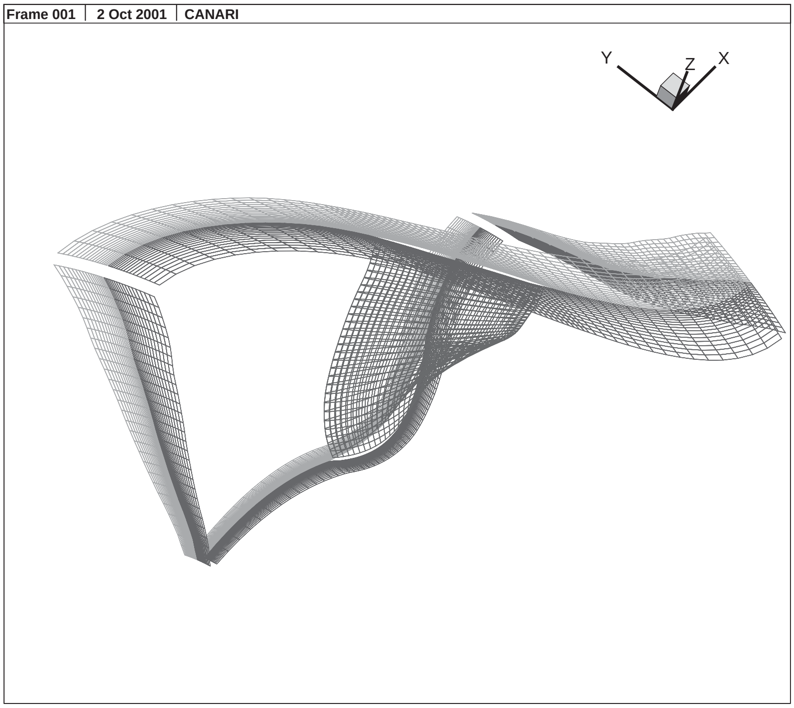

Fig. 1. Fluid mesh of the compressor blade.

Table 1
Coupling methods used for the test cases

Coupling method		Frequency domain	Time domain	Hypotheses
Indirect coupling	Double scanning	Cases 1, 2	No	Linearized aerodynamics, harmonic motion
	Smoothing	Case 2	Cases 1, 2	
Direct coupling		No	Case 1	

6.1. *Case 1:* $\Omega = 4066.4$ *r.p.m.*

This configuration is studied because of the availability of data resulting from a direct coupling numerical computation. The simulations have been performed for the following aerodynamic conditions:

$$\begin{cases} \text{rotation speed,} & \Omega = 4066.4 \text{ r.p.m.,} \\ \text{upstream total temperature,} & T_{i1} = 288 \text{ K,} \\ \text{upstream total pressure,} & P_{i1} = 101\,325 \text{ Pa,} \\ \text{pressure ratio,} & P_2/P_{i1} = 1.05, \\ \text{phase angle,} & \sigma_0 = 0^\circ. \end{cases}$$

The steady aerodynamic simulation gives for the inflow a Mach number of 0.5, a velocity of 166 m/s and a mass flow of 462.92 kg/s. Fig. 2, representing the steady pressure iso-surfaces on the boundaries of the domain, shows a shock whose position depends on the applied pressure ratio. The coupled simulations are then performed under transonic conditions.

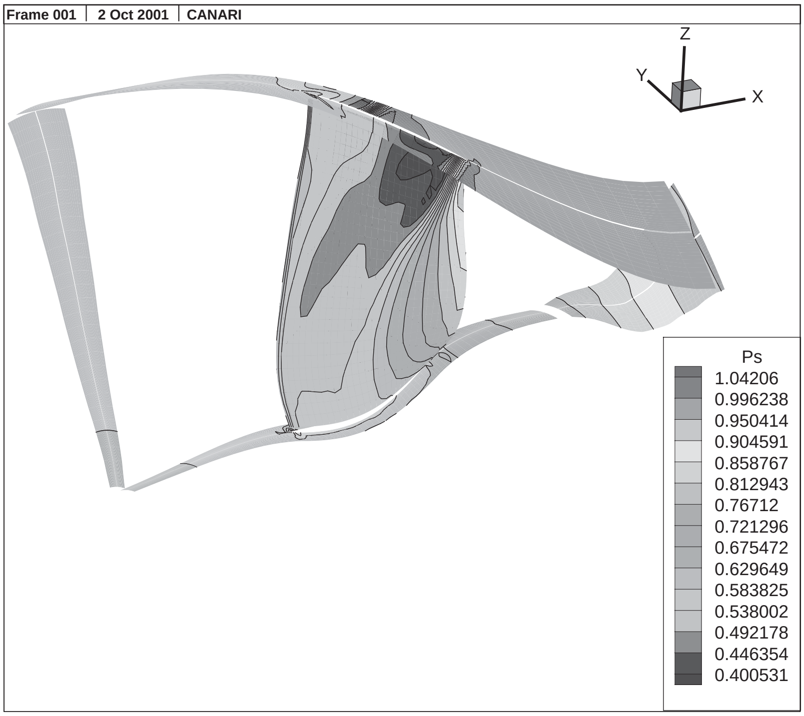

Fig. 2. Case 1—steady pressure.

Table 2
Case 1—excitation frequencies

Frequencies f (Hz)	5.28	79.25	97.4	105.7	184.9	204	211.3
Reduced frequencies $\kappa = 2\pi f/V_\infty$	0.2	3.0	3.69	4.0	7.0	7.72	8.0

For the coupling computation, only the first two bending modes of the blade whose frequencies are 97.4 Hz (1F) and 204.3 Hz (2F) are retained to form the projection basis. Unsteady aerodynamic simulations are performed using the mode shapes as oscillating motion shape for the frequencies given in Table 2.

For the coupling calculation, the blade is assumed not to have any structural damping. Fig. 3 shows the flutter diagram obtained using the double scanning method with both upstream infinite velocity and mass flow on the abscisses. No flutter can be seen in the upstream infinite velocity range from 130 to 250 m/s.

In order to perform a time simulation, a minimum state smoothing of the generalized aerodynamic forces is performed with a relative error of 0.197%. The time increment is determined to have 60 time steps per period (second mode). An initial velocity is applied to all generalized coordinates. Figs. 4 and 5 show the time evolution of both generalized coordinates computed using three methods: the first method is the indirect coupling in the time domain (smoothing method), the second one is a direct coupling numerical simulation using a grid deformation technique, and the last one is a direct coupling numerical simulation using a blowing condition. The results from the three methods are similar, although the aeroelastic damping computed with the direct simulation using the grid deformation technique is quite a lot smaller than those computed with the other methods. The good agreement between the results of the smoothing method and those of the direct coupling method with a blowing condition can be explained by the fact that the generalized aerodynamic forces used in the smoothing method was also computed with a blowing condition. Table 3 gives the frequencies and the damping factors computed using the three methods. Moreover, the results from the smoothing method in the time domain is similar to the one from the double scanning method in the frequency domain. The time simulation has been performed for an upstream infinite velocity $V_\infty = 166$ m/s.

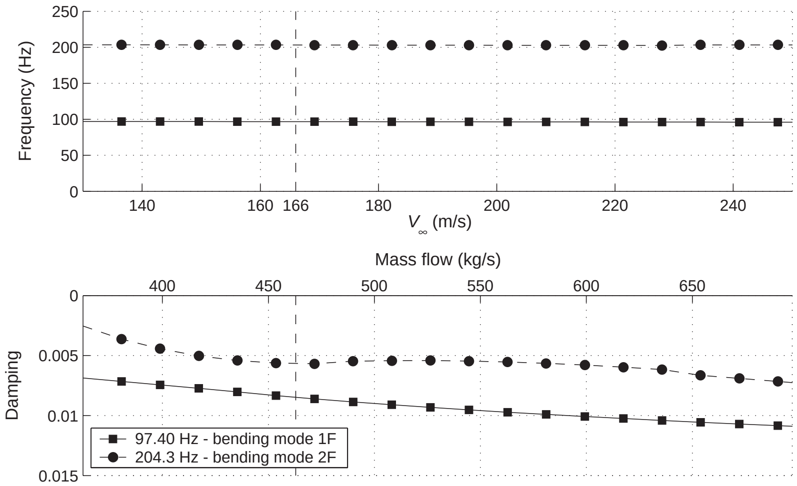

Fig. 3. Case 1—Flutter diagram (double scanning).

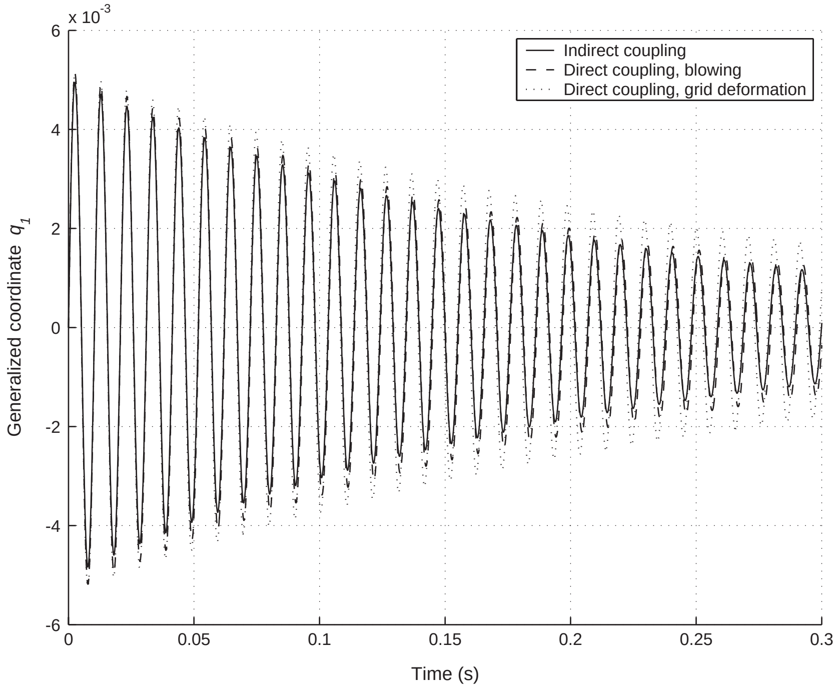

Fig. 4. Case 1—time evolution of q_1.

6.2. *Case 2:* $\Omega = 4516.8$ *r.p.m.*

A coupling calculation is performed on the same blade as previously at a higher rotation speed for two inter-blade phase angles, $\sigma_0 = 0^\circ$ and $\sigma_1 = 360^\circ/22$. The only changes in the aerodynamic conditions are:

$$\begin{cases} \text{rotation speed,} \;\; \Omega = 4516.8 \text{ r.p.m.,} \\ \text{pressure ratio,} \;\; P_2/P_{i1} = 1.12. \end{cases}$$

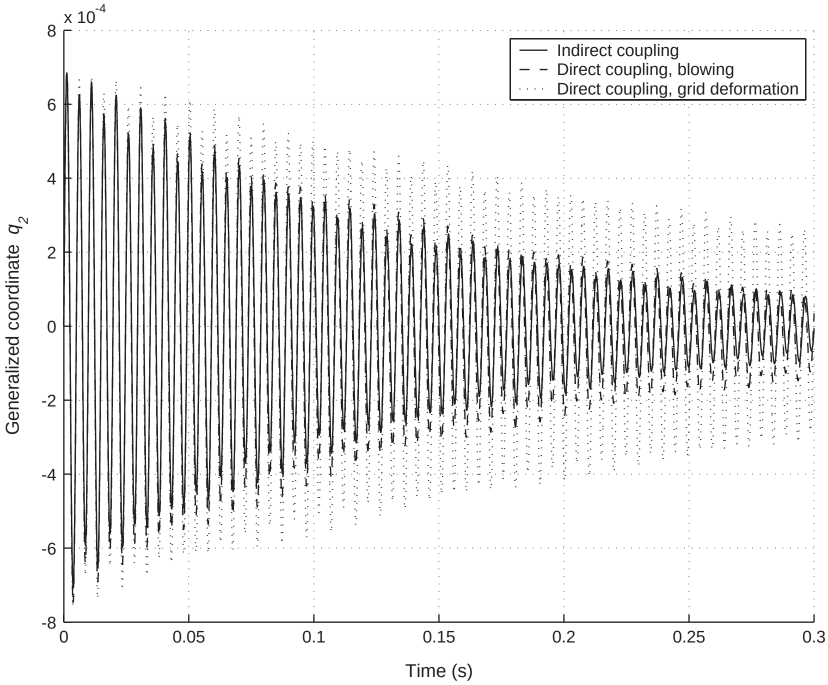

Fig. 5. Case 1—time evolution of q_2.

Table 3
Case 1—frequencies (Hz) and damping factors of q_1 and q_2 ($V_\infty = 166$ m/s)

	Time domain						Frequency domain	
	Smoothing		Direct (grid deform.)		Direct (blowing)		Double scanning	
	Frequency	Damping	Frequency	Damping	Frequency	Damping	Frequency	Damping
q_1	96.70	0.0082	96.94	0.0061	96.54	0.0077	96.69	0.0085
q_2	203.21	0.0056	203.47	0.0025	203.54	0.0048	203.13	0.0057

Table 4
Case 2, phase angle σ_0—excitation frequencies

Frequencies f (Hz)	0	5.0	70.0	101.7	230.1	448.9	600.0
Reduced frequencies $\kappa = 2\pi f/V_\infty$	0	0.185	2.59	3.755	8.5	16.58	22.16

For the inlet flow, the Mach number is 0.5, the velocity is 166 m/s and the mass flow is 487.95 kg/s. Like in the previous case, the coupled simulations are performed under transonic conditions.

A first coupling calculation is performed for an inter-blade phase angle $\sigma_0 = 0°$. The projection basis is formed by the first two bending modes and the first torsion modes whose frequencies are respectively 101.7 Hz (1F), 212.8 Hz (2F) and 448.9 Hz (1T). Unsteady generalized aerodynamic forces are computed at the frequencies given in Table 4.

The blade is still assumed to not have any structural damping. Figs. 6 and 7 show the flutter diagrams obtained with the double scanning and the smoothing methods. Both methods give similar results: the blade is stable in the upstream infinite velocity range from 100 to 250 m/s.

A time simulation is performed for an upstream infinite velocity $V_\infty = 166$ m/s with the minimum state smoothing method. The aerodynamic forces are approximated using 6 poles with a relative error of 1.13%. The time increment is

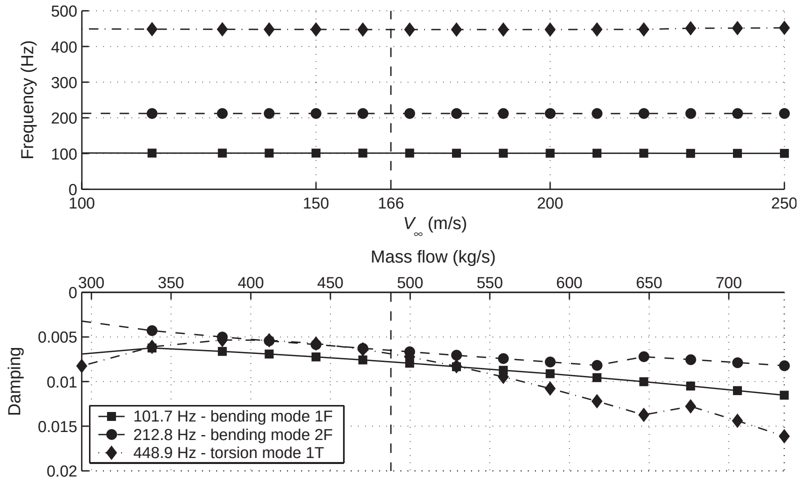

Fig. 6. Case 2, phase angle σ_0—flutter diagram (double scanning).

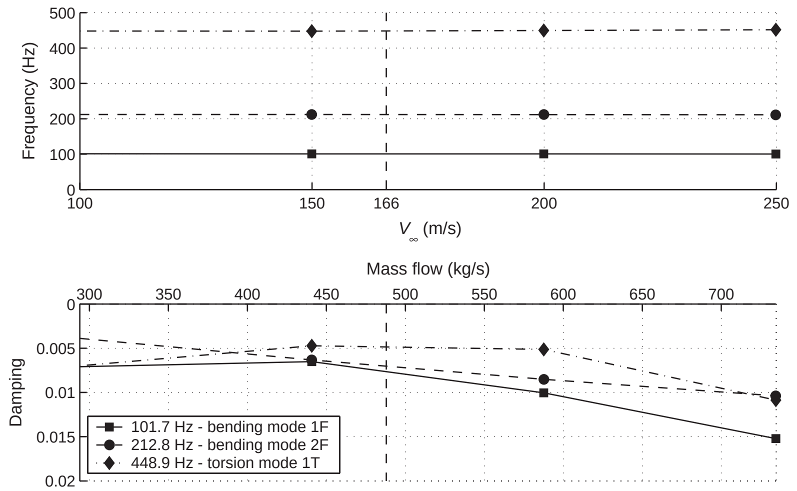

Fig. 7. Case 2, phase angle σ_0—flutter diagram (smoothing).

determined to have 60 time steps per period (third mode). Fig. 8 shows the time evolution of the three generalized coordinates q_1, q_2 and q_3. Table 5 shows a Fourier analysis of those signals. The resulting frequencies and damping factors are similar to those obtained from the computation in the frequency domain (double scanning method).

A coupling calculation is now performed for an inter-blade phase angle $\sigma_1 = 1 \times 360^\circ/22$. The method is then tested for a nonzero phase angle and for a complex projection basis. The latter is formed by the first two bending modes and the first torsion mode whose frequencies are respectively 105 Hz (1F), 191.8 Hz (2F) and 278.3 Hz (1T). Generalized aerodynamic forces are computed for the frequencies given in Table 6.

Fig. 9 shows the flutter diagram resulting from a computation using the double scanning method. As in the zero phase angle case, the blade is stable in the upstream infinite frequency range from 100 to 250 m/s.

A time calculation is performed for an upstream infinite velocity $V_\infty = 166$ m/s. The time increment is determined to have 60 time steps per period (third mode). The smoothing method uses 8 poles and gives a relative error of 1.18%. Figs. 10 and 11 show the time evolution of the three generalized coordinates. Table 7 shows the Fourier analysis of the signals. As for a zero phase angle, the frequencies and the damping factors resulting from the computations in the time domain (smoothing method) and in the frequency domain (double scanning method) are similar.

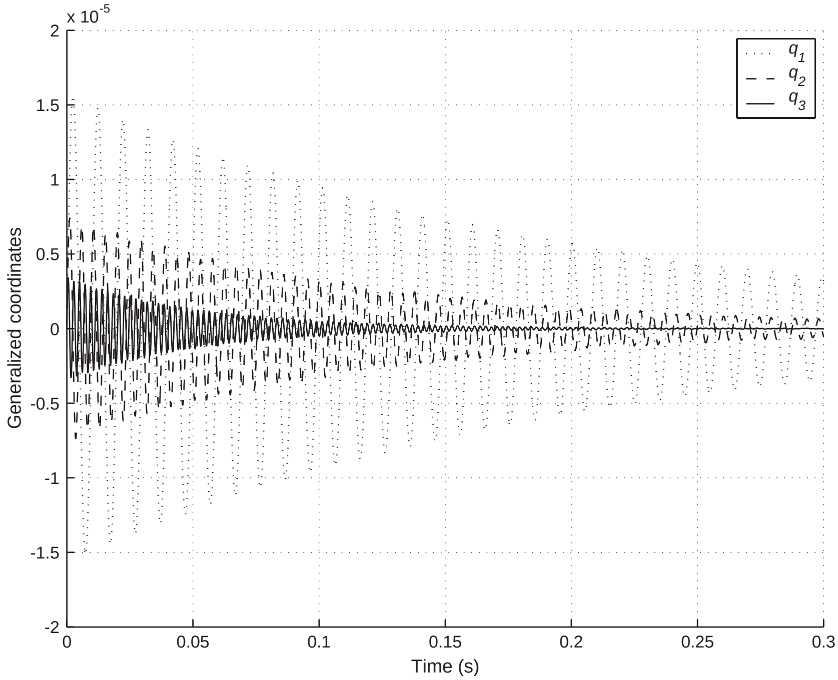

Fig. 8. Case 2, phase angle σ_0—time evolution of generalized coordinates.

Table 5
Case 2, phase angle σ_0—frequencies (Hz) and damping factors ($V_\infty = 166$ m/s)

	Time domain (Smoothing)		Frequency domain (Double scanning)	
	Frequency	Damping	Frequency	Damping
q_1	101.02	0.0080	100.96	0.0080
q_2	101.02	0.0080		
	212.18	0.0062	211.86	0.0063
q_3	101.02	0.0075		
	212.19	0.0069		
	447.00	0.0069	447.21	0.0073

Table 6
Case 2, phase angle σ_1—excitation frequencies

Frequencies f (Hz)	10.0	20.0	50.0	105.3	139	191.8	278.3	350.0
Reduced frequencies $\kappa = 2\pi f/V_\infty$	0.37	0.74	1.85	3.89	5.26	7.08	10.28	12.93

7. Conclusion

Two fluid–structure coupling methods for a rotating bladed disk system based on the cyclic symmetry properties and the projection on the complex modes are presented. The double scanning and the minimum state smoothing methods

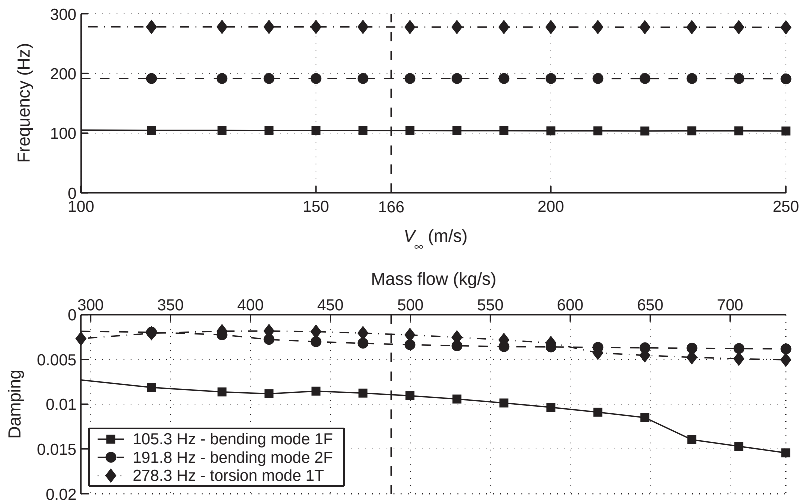

Fig. 9. Case 2, phase angle σ_1—flutter diagram (double scanning).

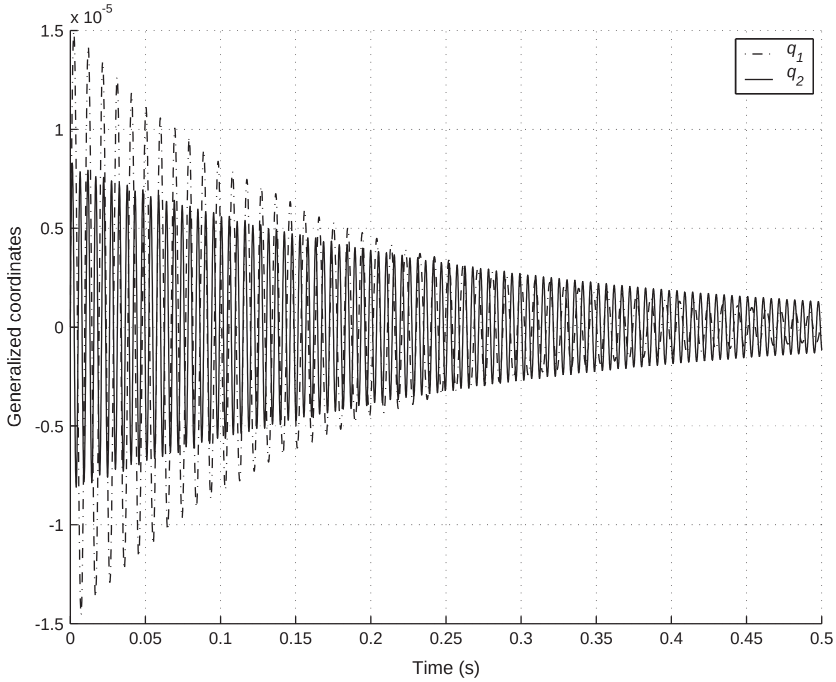

Fig. 10. Case 2, phase angle σ_1—time evolution of q_1 and q_2.

can both be used for solving the flutter equation in the frequency domain, while the time response is computed by modelling the generalized aerodynamic forces using the minimum state smoothing method. The proposed methods are tested on a compressor blade row in order to determine the aeroelastic stability of the system in function of the velocity or the mass flow of the upstream unperturbed fluid. In the velocity range of interest around the nominal value, both frequency-domain methods provide similar aeroelastic frequencies and damping factors. These latter also correspond to the ones obtained from the time-domain simulation and from the direct coupling method.

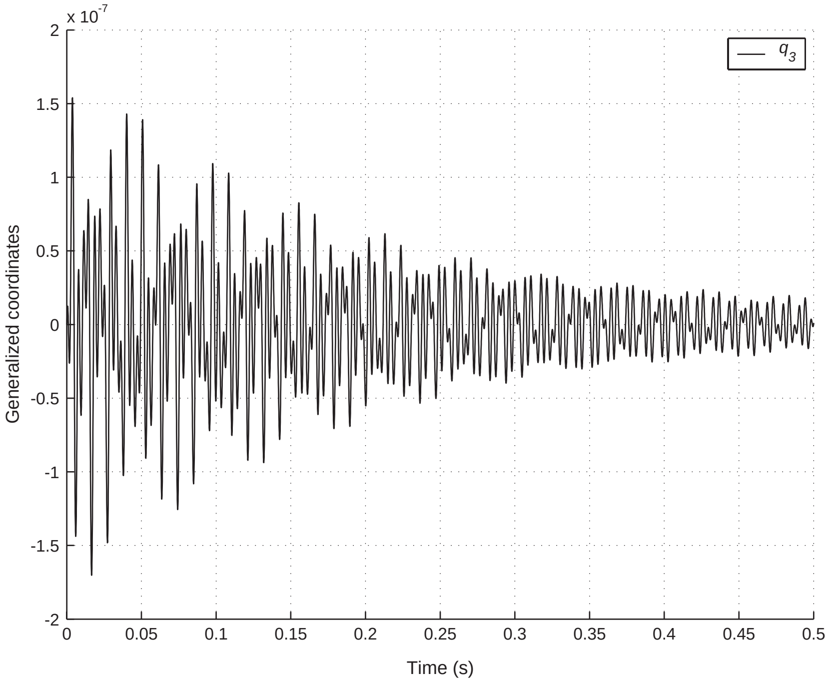

Fig. 11. Case 2, phase angle σ_1—time evolution of q_3.

Table 7
Case 2, phase angle σ_1—frequencies (Hz) and damping factors ($V_\infty = 166$ m/s)

	Time domain (smoothing)		Frequency domain (Double scanning)	
	Frequency	Damping	Frequency	Damping
q_1	104.92	0.0092	104.14	0.0091
q_2	104.21	0.0092		
	191.34	0.0031	191.42	0.0034
q_3	104.23	0.0089		
	191.35	0.0031		
	277.40	0.0022	277.73	0.0023

The double scanning method is more robust but it is only applicable for solving the flutter equation in the frequency domain. The minimum state smoothing method can be used for both frequency and time domain simulations but its implementation is more complex and it requires more attention and know-how from the user. The main advantage of the proposed indirect coupling method in the time domain is that it is generally less time consuming than the direct coupling method since the aerodynamic calculations are performed only once at the beginning of the simulation and not at each time step. Therefore, the aerodynamic forces do not need to be computed again if the modes that generate them are unchanged and they can be re-used for other computations, for example when the applied external forces change or when we want to study the influence of a friction damper on the stability of the bladed disk. However, the proposed indirect coupling method is more restrictive and less accurate since it is based on the assumptions of linearized aerodynamics and harmonic motion, which is not the case of the direct coupling method.

The good agreement between the results of the different methods shows that the extension of the proposed coupling methods from aircraft applications to turbomachinary is feasible. However, further validation tests should be carried out under various conditions such as other rotation speeds, phase angles, pressure ratios, viscous fluid, etc.

The future work will consist in: numerical simulations of an unstable configuration with comparison to experimental results in order to test the flutter prediction capability; numerical simulations with structural nonlinearities such as free-play or friction by using the Craig and Bampton projection basis; the introduction of the mistuning of the blades, in which case the cyclic symmetry properties are no longer applicable and model reduction methods such as component mode synthesis will be used instead.

Appendix A. Approximation of the aerodynamic coefficient matrix

This appendix describes the computation of the matrices $\mathbf{A}_{n0}, \mathbf{A}_{n1}, \mathbf{A}_{n2}, \mathbf{D}_n, \mathbf{R}_n$ and $\mathbf{E}_n$ in the approximation equation (48) of the aerodynamic coefficient matrix $\tilde{\mathbf{A}}_n$ from the tabulated matrices $\tilde{\mathbf{A}}_n(\mathbf{\Phi}_n, \mathrm{i}\kappa)$ obtained for n_κ reduced frequencies $\kappa = \kappa_1, \ldots, \kappa_{n_\kappa}$. This is done by using a method of least squares minimization (Poirion, 1995).

For each (i,j)-term of the matrix $\tilde{\mathbf{A}}_n$, we define the error ε_{ij}, for $i,j = 1, \ldots, m_n$:

$$\varepsilon_{ij} = \frac{1}{M_{ij}} \sum_{k=1}^{n_\kappa} |w_{ij,k}[\tilde{\mathbf{A}}_n(\mathbf{\Phi}_n, \mathrm{i}\kappa_k) - \mathbf{A}_{n0} - (\mathrm{i}\kappa_k)\mathbf{A}_{n1} - (\mathrm{i}\kappa_k)^2\, \mathbf{A}_{n2} - (\mathrm{i}\kappa_k)\mathbf{D}_n[(\mathrm{i}\kappa_k)\mathbf{I} - \mathbf{R}_n]^{-1}\mathbf{E}_n]_{ij}|^2,$$

where $M_{ij} = \max_{k=1}^{n_\kappa}(1, |\tilde{\mathbf{A}}_{n,ij}(\mathbf{\Phi}_n, \mathrm{i}\kappa_k)|^2)$ and $w_{ij,k}$ are normalization coefficients which allow some reduced frequencies or some modes to be privileged compared to the others.

The following steps are performed:

(i) put $\mathbf{A}_{n0} = \tilde{\mathbf{A}}_n(\mathbf{\Phi}_n, 0)$, the steady state aerodynamic coefficient matrix obtained with the reduced frequency equal to zero;
(ii) choose arbitrarily the matrix $\mathbf{D}_n$, the number of poles n_p and the negative poles $r_1, \ldots, r_{n_p}$ which are the terms of the diagonal matrix $\mathbf{R}_n$;
(iii) for successively each value of $j = 1, \ldots, m_n$ and with $\mathbf{D}_n$ fixed, compute the jth columns of $\mathbf{A}_{n1}, \mathbf{A}_{n2}$ and $\mathbf{E}_n$, which are the solutions of m_n simultaneous least-squares problems which minimize ε_{ij} for $i = 1, \ldots, m_n$ (linear system of $(2+n_p)m_n$ equations and $2m_n + n_p$ unknowns);
(iv) for successively each value of $i = 1, \ldots, m_n$ and with $\mathbf{E}_n$ fixed, compute the ith rows of $\mathbf{A}_{n1}, \mathbf{A}_{n2}$ and $\mathbf{D}_n$, which are the solutions of m_n simultaneous least-squares problems which minimize ε_{ij} for $j = 1, \ldots, m_n$ (linear system of $(2+n_p)m_n$ equations and $2m_n + n_p$ unknowns);
(v) repeat steps 3 and 4 until the convergence on the cost function $J = (\sum_{ij} \varepsilon_{ij})^{1/2}$ is obtained.

The method can diverge, depending on the initial values of the poles. The latter are generated at random while the number of poles n_p should be at least $m_n + 1$.

Appendix B. Fixed point method for nonlinear eigenvalue problem

This appendix describes the iterative process of the fixed point method for finding the eigensolutions $(p, \mathbf{x})$ the nonlinear eigenvalue problem Eq. (50) for n_V increasing velocities $V_\infty^1, \ldots, V_\infty^{n_V}$. For each velocity V_∞^k, the following eigenvalue problems are solved for $i = 1, \ldots, 2m_n$ and $j = 0, 1, 2, \ldots,$ until convergence on p_i is obtained:

$$\mathbf{H}(p_{i,j})\mathbf{x}_{i,j+1} = p_{i,j+1}\mathbf{x}_{i,j+1},$$

where $(p_{i,j}, \mathbf{x}_{i,j})$ is the ith eigensolution obtained at the jth iteration. The eigensolutions obtained for V_∞^k will be used as the initialization of the iterative process for V_∞^{k+1}. The initialization for V_∞^1 is the solution of Eq. (50) in vacuum in which case the iterative process is not necessary.

Let us suppose that the eigensolutions for $V_\infty^1, \ldots, V_\infty^k$ and the first i eigensolutions $(p_1^{k+1}, \mathbf{x}_1^{k+1}), \ldots, (p_i^{k+1}, \mathbf{x}_i^{k+1})$ for V_∞^{k+1} have been obtained and we are now computing the $(i+1)$th eigensolution. The iteration process starts with $p_{i+1,0}^{k+1} = p_{i+1}^k$, the $(i+1)$th eigenvalue obtained for V_∞^k. At the jth iteration, the following operations are done:

(i) computation of the eigensolutions $(p_{1,j}^{k+1}, \mathbf{x}_{1,j}^{k+1}), \ldots, (p_{2m_n,j}^{k+1}, \mathbf{x}_{2m_n,j}^{k+1})$ of $\mathbf{H}(p_{i+1,j-1}^{k+1})$;
(ii) eigenvector follow-up procedure which consists in finding out the eigenvector $\mathbf{x}_{l,j}^{k+1}$ which minimizes the distance to $\mathbf{x}_{i+1}^k$, the $(i+1)$th eigenvector obtained for V_∞^k, i.e., $\mathbf{x}_{l,j}^{k+1}$ should satisfy $|\langle \mathbf{x}_{l,j}^{k+1}, \mathbf{x}_{i+1}^k \rangle| = \max_{l'=1}^{2m_n} |\langle \mathbf{x}_{l',j}^{k+1}, \mathbf{x}_{i+1}^k \rangle|$, the eigenvectors having unit norm (with the scalar product $\langle \mathbf{x}, \mathbf{y} \rangle = {}^t\bar{\mathbf{x}}\mathbf{y}$ and the norm $\|\mathbf{x}\| = \sqrt{{}^t\bar{\mathbf{x}}\mathbf{x}}$);
(iii) test on the selected eigenvalue $p_{l,j}^{k+1}$ to verify that it does not correspond to one of the first i eigenvalues previously found, i.e., it should satisfy $\min_{l'=1}^{i}(|p_{l,j}^{k+1} - p_{l'}^{k+1}|/|p_{l,j}^{k+1}|) > \varepsilon_1$. Otherwise, $p_{l,j}^{k+1}$ was already found, the lth eigensolution is eliminated and step 2 is repeated;

(iv) the $(i+1)$th eigensolution at the jth iteration being selected, test on the convergence of the eigenvalue; the iterative process will stop if $|p_{i+1,j}^{k+1} - p_{i+1,j-1}^{k+1}|/|p_{i+1,j}^{k+1}| \leqslant \varepsilon_2$;

(v) if the convergence is slow, the eigenvalue can be updated by a relaxation technique by using $c_r p_{i+1,j}^{k+1} + (1-c_r)p_{i+1,j-1}^{k+1}$ instead of $p_{i+1,j}^{k+1}$ for computing the matrix $\mathbf{H}(p)$ in the next iteration, where $c_r \in [0,1]$ is the relaxation coefficient.

References

Bathe, K.-J., 1996. Finite Element Procedures. Prenctice-Hall, Upper Saddle River, NJ.

Berthillier, M., Dhainaut, M., Burgaud, F., Garnier, V., 1997. A numerical method for the prediction of bladed disk forced response. Journal of Engineering for Gas Turbines and Power 119, 404–410.

Berthillier, M., Dupont, C., Chanez, P., Saurat, F., 1998. Réponse forcée aéroélastique des aubes de turbomachines. Bulletin SFM, Revue Française de Mécanique (4), 265–275.

Brillouin, L., 1946. Wave Propagation in Periodic Structures. International Series in Pure and Applied Physics. McGraw-Hill Book Company, Inc., New York, London.

Craig Jr., R.R., Bampton, M.C.C., 1968. Coupling of substructures for dynamic analysis. AIAA Journal 6, 1313–1319.

Crawley, E.F., 1988. Aeroelastic formulation for tuned and mistuned rotors. AGARD-AG-298, Vol. 2, pp. 19.1–19.24.

Dat, R., Meurzec, J.-L., 1969. Sur les calculs de flottement par la méthode dite du "balayage en fréquence réduite". La Recherche Aérospatiale (133), 41–43.

Dugeai, A., Madec, A., Sens, A.S., 2000. Numerical unsteady aerodynamics for turbomachinery aeroelasticity. In: Proceedings of the 9th International Symposium on Unsteady Aerodynamics, Aeroacoustics and Aeroelasticity of Turbomachines, Lyon, pp. 830–840.

Elhami, A., Lallement, G., Minotti, P., Cognan, S., 1993. Methods that combine finite group theory with component mode synthesis in the analysis of repetitive structures. Computers & Structures 48, 975–982.

Farhat, C., Lesoinne, M., Maman, N., 1995. Mixed explicit/implicit time integration of coupled aeroelastic problems: three-field formulation, geometric conservation and distributed solution. International Journal for Numerical Methods in Fluids 21, 807–835.

Géradin, M., Kill, K., 1986. A three dimensional approach to dynamic analysis of rotating shaft disc flexible systems. In: Proceedings of the Second International Conference on Rotordynamics IFToMM, Tokyo, pp. 87–93.

Grisval, J.-P., Liauzun, C., 1999. Application of the finite element method to aeroelasticity. Revue Européene des Éléments Finis 8, 553–579.

Grisval, J.P., Liauzun, C., 2000. Unsteady viscous flow in turbomachinery cascade: a finite element approach. In: Proceedings of the 8th International Symposium on Transport Phenomena and Dynamics of Rotating Machinery, ISROMAC-8, Vol. 1, Hawaii, pp. 407–412.

Henry, R., 1980. Calcul des fréquences et modes des structures répétitives circulaires. Journal de Mécanique Appliquée 4, 61–82.

Jacquet-Richardet, G., Dal-Ferro, C., 1995. Analyse du comportement dynamique des roues de turbomachines immergées. Revue Européene des Éléments Finis 4, 441–465.

Jacquet-Richardet, G., Henry, R., 1994. A modal aeroelastic finite element analysis method for advanced turbomachinery stages. International Journal for Numerical Methods in Engineering 37, 4205–4217.

Jacquet-Richardet, G., Rieutord, P., 1998. A three-dimensional fluid–structure coupled analysis of rotating flexible assemblies of turbomachines. Journal of Sound and Vibration 209, 61–76.

Jacquet-Richardet, G., Ferraris, G., Rieutord, P., 1996. Frequencies and modes of rotating flexible bladed disc-shaft assemblies: a global cyclic symmetry approach. Journal of Sound and Vibration 191, 901–915.

Jameson, A., Schmidt, W., Turkel, E., 1981. Numerical solutions of the Euler equations by finite volume methods using Runge–Kutta time-stepping schemes. In: AIAA 14th Fluid and Plasma Dynamics Conference, Palo Alto, CA, AIAA-81-1259.

Karpel, M., 1982. Design for active flutter suppression and gust alleviation using state-space aeroelastic modeling. AIAA Journal of Aircraft 19, 221–227.

Karpel, M., 1990. Time-domain aeroservoelastic modeling using weighted unsteady aerodynamic forces. Journal of Guidance, Control, and Dynamics 13, 30–37.

Lalanne, B., Touratier, M., 1998. Linearized approach of fluid-structure vibrations in cyclic symmetric domains. In: Proceedings of the Seventh International Symposium on Rotating Machinery, Hawaii.

Lalanne, B., Touratier, M., Desmaison, T., 1998. Formulation linéarisée des problèmes couplés de vibrations dans les turbomachines. Bulletin SFM, Revue Française de Mécanique (2), 81–88.

Maman, N., Farhat, C., 1995. Matching fluid and structure meshes for aeroelastic computations: a parallel approach. Computers & Structures 54, 779–785.

Marshall, J.G., Imregun, M., 1996. Review of aeroelasticity methods with emphasis on turbomachinery applications. Journal of Fluids and Structures 10, 237–267.

Mastroddi, F., Gennaretti, M., 2001. An investigation about finite-state models for aeroelastic analysis of fixed wings. In: Proceedings of the International Forum on Aeroelasticity and Structural Dynamics IFASD 2001, Vol. 2, Madrid, Spain, pp. 273–286.

Mead, D.J., 1975. Wave propagation and natural modes in periodic systems: I—mono-coupled systems. II—multicoupled systems with and without damping. Journal of Sound and Vibration 40, 1–39.

Mézière, L., 1994. Vibrations de structures à symétrie cyclique: application au cas des turbomachines. AGARD-CP-537, Vol. 1, pp. 37.1–37.9.

Miller, A.G., 1981. Application of group representation theory to symmetric structures. Applied Mathematical Modelling 5, 290–294.

Newmark, N.M., 1959. A method of computation for structural dynamics. ASCE Journal of Engineering Mechanics Division 8, 67–94.

Orris, R.M., Petyt, M., 1974. A finite element study of harmonic wave propagation in periodic structures. Journal of Sound and Vibration 33, 223–236.

Poirion, F., 1995. Modélisation temporelle des systèmes aéroservoélastiques. Application à l'étude des effets des retards. La Recherche Aérospatiale (2), 103–114.

Roberts, R.P., 1991. The application of the minimum state method for approximating unsteady aerodynamics to an aircraft model. In: Proceedings of the European Forum on Aeroelasticity and Structural Dynamics, Aachen.

Sayma, A.I., Vahdati, M., Imregun, M., 2000. An integrated nonlinear approach for turbomachinery forced response prediction. Part I: Formulation. Journal of Fluids and Structures 14, 87–101.

Thomas, D.L., 1979. Dynamics of rotationally periodic structures. International Journal for Numerical Methods in Engineering 14, 81–102.

Tran, D.-M., 2000. A comparison of component mode synthesis methods for cyclic structures. In: Han, R.P.S., Lee, K.H., Luo, A.C.J. (Eds.), Dynamics, Acoustics and Simulations. 2000 ASME International Mechanical Engineering Congress and Exposition, Vol. DE-108, DSC-68, Orlando, FL, pp. 23–30.

Tran, D.-M., 2001. Component mode synthesis method using interface modes. Application to structures with cyclic symmetry. Computers & Structures 79, 209–222.

Tran, D.-M., Labaste, C., Liauzun, C., 2001. Method of fluid structure coupling in frequency domain for turbomachineries. In: Cheng, L., Li, K.M., So, R.M.C. (Eds.), Proceedings of the Eighth International Congress on Sound and Vibration ICSV8. The Hong Kong Polytechnic University, Hong Kong, China, pp. 571–578.

Valid, R., Ohayon, R., 1985. Théorie et calcul statique et dynamique des structures à symétries cycliques. La Recherche Aérospatiale (4), 251–263.

Wildheim, S.J., 1979. Excitation of rotationally periodic structures. Journal of Applied Mechanics 46, 878–882.